

# NUMERICAL MODELING OF MOIST CONVECTION IN JUPITER'S ATMOSPHERE AND FUTURE JUPITER PROBE MISSION

K. Sugiyama<sup>1</sup>, M. Odaka<sup>1</sup>, K. Nakajima<sup>2</sup>, and Y.-Y. Hayashi<sup>3</sup>

<sup>1</sup>Dep. of CosmoSciences, Hokkaido Univ. (Kita-10 Nishi-8 Kita-ku, Sapporo 060-0810, Japan),  
sugiyama@gfd-dennou.org, odakker@gfd-dennou.org,

<sup>2</sup>Dep. of Earth and Planetary Sciences, Kyushu Univ. (6-10-1 Hakozaki, Higashi-ku, Fukuoka 812-8581, Japan),  
kensuke@geo.kyushu-u.ac.jp

<sup>3</sup>Dep. of Earth and Planetary Sciences, Kobe Univ. (1-1 Rokkodai-cho, Nada-ku, Kobe, 657-8501, Japan),  
shosuke@gfd-dennou.org

## Abstract

We develop a two-dimensional fluid dynamical model that incorporates condensation of  $H_2O$  and  $NH_3$  and the production reaction of  $NH_4SH$ . We run the model for a long simulation time in order to examine the structure of moist convection layer in Jupiter's atmosphere established through a large number of life cycles of convective clouds with strong radiation. Our results show that  $H_2O$  and  $NH_4SH$  cloud particles are advected to altitudes above the  $NH_3$  condensation level. The convective motion and the distribution of condensible species depend on the deep tropospheric mixing ratios of condensible volatiles. Some suggestions for future probe missions will be given.

## 1. Introduction

Cloud convection is supposed to play important roles in shaping large scale circulation and distributions of condensible species [1] [2]. However, the cloud convective motion and the distribution of condensible species in Jupiter's atmosphere has not been clarified yet, especially because direct measurement is taken only by Galileo probe and it is difficult to observe those under the surface cloud layer by remote sensing.

In previous studies, the vertical profiles of clouds in Jupiter's atmosphere has been investigated by using Equilibrium Cloud Condensation Model (ECCM) [3] [4] where adiabatic ascend of air parcel and its thermodynamic equilibrium are supposed. These studies predict the existence of three cloud layers;  $H_2O$  liquid/ice layer in the deepest, solid  $NH_4SH$  layer in the middle, and the uppermost  $NH_3$  ice layer (see Fig.1). However, the vertical profiles of clouds in Jupiter's atmosphere should surely be somewhat different from those expected by ECCMs, because adiabatic ascend of air parcel is not always maintained through the entire atmospheric column and convective motion and the microphysical processes, e.g. precipitation, should modify the profiles of clouds.

Recently, some studies on moist convection in Jupiter's atmosphere are performed by using numerical model

where vertical convective motion is represented explicitly and cloud microphysics of condensible volatiles are considered [5] [6]. However, their main interest is to simulate a life cycle of a single cloud; the convective motion and the distribution of condensible species that are established through a large number of life cycles of convective clouds are out of their focus. Moreover, all of the condensible volatiles in Jupiter's atmosphere are not considered in their models.

A precursor study on the convective motion and the distribution of condensible species in Jupiter's atmo-

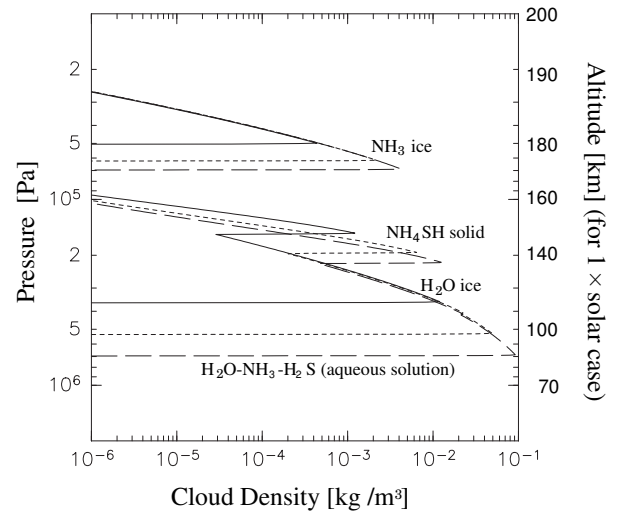


Figure 1. Vertical profiles of cloud density determined by an Equilibrium Cloud Condensation Model (ECCM). The abundance of condensible elements in the deep troposphere are taken at  $1 \times$  solar (solid line),  $5 \times$  solar (dotted line),  $10 \times$  solar (broken line). The solar abundance is adopted from Asplund et al. [7]. Altitude which is calculated by hydrostatic equilibrium equation for  $1 \times$  solar case is also shown. The zero of altitude is at  $3 \times 10^6$  Pa level. This calculation is performed by using the code which developed in Sugiyama et al. [8].

sphere that are established through a large number of life cycles of convective clouds is Nakajima *et al.* [9]. They examine those by using a two-dimensional model which incorporates H<sub>2</sub>O condensation only. The results show that the stable layer associated with H<sub>2</sub>O condensation distinctively separates vertical convective motion. Therefore, the NH<sub>3</sub> cloud and NH<sub>4</sub>SH cloud, which are not considered in their model, may also affect convection structure, because the latent heat of NH<sub>3</sub> and reaction heat of NH<sub>4</sub>SH alter the vertical profile of stability. In fact, peak values of the static stability associated with NH<sub>3</sub> condensation and NH<sub>4</sub>SH production evaluated from the difference between moist and dry adiabats reaches 1/3 and 1/5 of that associated with H<sub>2</sub>O condensation, respectively [8].

We are now developing a two-dimensional moist convection model that incorporates condensation of H<sub>2</sub>O and NH<sub>3</sub> and production reaction of NH<sub>4</sub>SH, and performing simulations with a fixed thermal forcing in order to examine the convective motion and distribution of condensible species in Jupiter's atmosphere. In this paper, we present our numerical model, results of simulations of moist convection in Jupiter's atmosphere, and some suggestions for future probe missions to Jupiter.

## 2. Numerical Model

The basic equations of the model is based on the quasi-compressible system which is developed for the simulation of terrestrial convective clouds [10]. The cloud microphysics is implemented by using the warm rain bulk parameterization [11] that is widely used in the modeling studies on the terrestrial cloud convection. In this parameterization, each condensible species is divided into three categories "vapor", "cloud", and "rain"; both rain and cloud are condensed phase, but rain falls down relative to the air, whereas cloud does not. The conversion rates between each categories are calculated by using the bulk mixing ratios of the three categories of condensible components (see Fig.2). Vapor is converted to cloud when saturation condition is met, and cloud is further converted to rain. The conversion rate due to collection and the fall velocity of rain is specified as three times the value used in terrestrial case [9]. The time constant of autoconversion of the rain is 100 sec and its critical cloud mixing ratio is set to zero [9]. We assume that the categories of cloud and rain consist of pure condensible species; solution is not considered. The subgrid scale turbulence is implemented by using the parameterization [10] in which the eddy mixing coefficients are diagnosed from the subgrid kinetic energy that is predicted by a prognostic equation. The radiative transfer in Jupiter's atmosphere is not explicitly solved. Instead, the model atmosphere is subject to a thermal forcing which drive the convection.

## 3. Set-up of Experiment

The domain extends 300 km (30 bar – 0.001 bar) in the vertical direction and 512 km in the horizontal direction. Cyclic boundary condition is assumed in the horizontal direction. At the top and the bottom boundaries, stress

free boundary condition and  $w = 0$  are assumed. Temperature and mixing ratios of condensible volatiles are fixed at the bottom boundary. The spatial resolution is 2 km both in the horizontal and the vertical directions.

The initial vertical profile of the atmosphere is as follows: the atmosphere consists of an isentropic "troposphere" below and an isothermal "stratosphere" above. The troposphere (the temperature at 0.6 Bar is 160 K) extends up to  $z = 200$  km (0.1 bar), and the temperature of the stratosphere above is 100 K. Random potential temperature perturbation ( $\Delta\theta = 0.1$  K) is given at 110 km level to seed convective motion.

H<sub>2</sub> and He are treated as dry (non condensible) components, and their abundances are specified at the solar abundance. The value of solar abundance is adopted from Asplund *et al* [7]. On the other hand, H<sub>2</sub>O, NH<sub>3</sub>, and NH<sub>4</sub>SH are considered as condensible components, and deep atmospheric abundances of condensible components are specified to be the solar abundance in the standard experiment. We also performed two additional cases where the deep abundances of all of the three condensible components are increased or decreased by a common factor. In the "10 times solar" case, the deep abundances of H<sub>2</sub>O, NH<sub>3</sub>, and NH<sub>4</sub>SH are all enhanced by ten times, whereas they are depleted by ten times in the "0.1 times solar" case. The initial mixing ratio of each condensible species is homogeneous below the level where the relative humidity reaches 75 %. In the altitudes above that level, the mixing ratio of each condensible components is reduced so that the relative humidity does not exceed 75 %.

The model atmosphere is subject to a thermal forcing which drive the convection between 2 bar level and 0.1 bar level where Galileo probe measures radiative cooling [12]. The cooling rate in the present study,  $-1$  K/day, is about 100 times larger than that appropriate for Jupiter's atmosphere compared with the estimated thermal relaxation time of several years [12]. However, if the actual parameters are used, the CPU time required for the establishment of the atmospheric structure is very long (a few years). We use such strength of thermal forcing in order to accelerate the establishment of the convective motion and the distribution of condensible species.

The time integration is continued up to about 1,400 hours, which is much longer than the time scale of each clouds. At the final stage, equilibration of the atmospheric structure seems to be established.

## 4. Results

### 4.1. Result of 1 times solar case

Hereafter, for simplicity, we will not mention cloud and rain separately; we will refer sum of mixing ratios of category "cloud" and "rain" as "cloud mixing ratio".

Fig.3 (a) shows the distributions of clouds of H<sub>2</sub>O, NH<sub>4</sub>SH and NH<sub>3</sub>. Clouds are far from homogeneous between the H<sub>2</sub>O condensation level and the tropopause. H<sub>2</sub>O and NH<sub>4</sub>SH cloud particles are advected upward up to altitude above the NH<sub>3</sub> condensation level at the region where active convective motion is occurred. This characteristics is obviously different from the static three

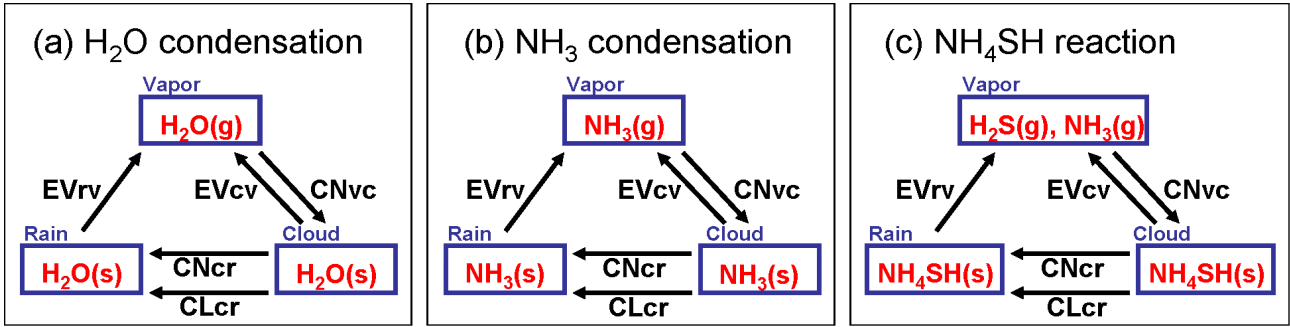


Figure 2. Schematic figure of the cloud microphysics parameterization for condensation of H<sub>2</sub>O (a) and NH<sub>3</sub> (b), and for production reaction of NH<sub>4</sub>SH (c). “CN<sub>vc</sub>” means condensation or reaction from vapor to cloud, “EV<sub>cv</sub>” means evaporation from cloud to vapor, “EV<sub>rv</sub>” means evaporation from rain to vapor, “CN<sub>cr</sub>” means autoconversion from cloud to rain, and “CL<sub>cr</sub>” means collection from cloud to rain.

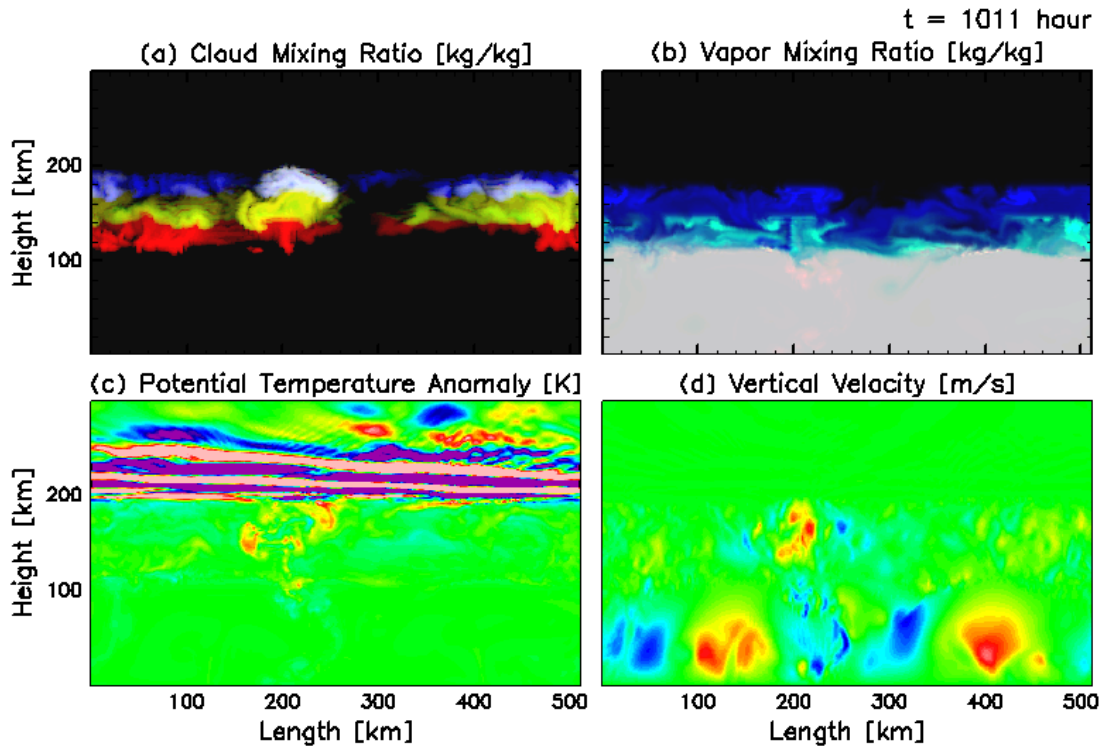


Figure 3. Snapshot of simulated cloud mixing ratios (a), mixing ratios of condensible volatiles (b), potential temperature anomaly from horizontal average (c), and vertical velocity (d) in the entire domain for the  $1 \times$  solar case. Cloud mixing ratios are represented by logarithmic scale ranging from  $10^{-8}$  to  $5 \times 10^{-4}$  kg/kg. Images in H<sub>2</sub>O ice (red), in NH<sub>4</sub>SH ice (green), in NH<sub>3</sub> ice (blue) are superposed. Mixing ratios of condensible volatiles are presented by linear scale nomalized by initial values. Images in H<sub>2</sub>O vapor (red), in H<sub>2</sub>S vapor (green), in NH<sub>3</sub> vapor (blue) are superposed. Potential temperature anomaly is represented by linear scale ranging from -2 to 2 K. Vertical velocity is represented by linear scale ranging from -60 to 60 m/s.

layers structure that has been expected by using equilibrium cloud condensation models. Time evolution (not shown here) reveals that the convective clouds develop and disappear in various locations with life time of a few hours.

Fig.3 (b) shows the distribution of condensible volatiles. Below the  $H_2O$  condensation level, mixing ratios of condensible volatiles are almost homogeneous. Above the  $H_2O$  condensation level, the distributions of these mixing ratios are horizontally inhomogeneous. Each condensible volatiles is saturated in the convective clouds, while the regions of downward motion are much drier. In some regions, extremely dry airs come down from the tropopause, but they stop to descend at the  $H_2O$  condensation level.

The vertical profiles of time and horizontal mean mixing ratios of condensible volatiles are shown Fig.4. These mixing ratios are almost constant below the  $H_2O$  condensation level, while they decrease upward above the  $H_2O$  condensation level. The profiles of mixing ratios of  $NH_3$  and  $H_2S$  are different from those expected by using equilibrium cloud condensation models. Instead of the sharp decrease at the corresponding condensation level predicted by the equilibrium cloud condensation models, they decrease much more smoothly from below to above the condensation levels in the present experiment.

Fig.3 (c) shows the distribution of potential temperature deviation from the initial profile. The convective clouds are warmer than their environment. Potential temperature is almost homogeneous below the  $H_2O$  condensation level, except for the cold plume below the convective cloud, which results from the evaporation of rain that fall down from the cloud above.

Fig.3 (d) shows the distribution of vertical velocity. Convective motion is distinctively separated at the  $H_2O$  condensation level at  $z = 120$  km. The distribution below the  $H_2O$  condensation level is characterized with regular upward and downward motions. The air motion above the  $H_2O$  condensation level is irregular corresponding to the intermittent developments of convective clouds. Strong updrafts are found in the  $H_2O$  convective clouds. These characteristics are common to the results of Nakajima *et al.* [9] which consider  $H_2O$  condensation only. Contrarily to the anticipation we presented in the introduction, neither  $NH_3$  condensation level (about  $z = 180$  km) nor  $NH_4SH$  production level (about  $z = 150$  km) acts as very distinct dynamical boundary. However, close examination reveals the frequent occurrence of small scale updrafts and downdrafts near these levels.

Fig.5 shows the time and horizontal mean thermal budget. The solid line in Fig.5 represents the contribution of the latent heat of condensation (or evaporation) of  $H_2O$  and  $NH_3$  and the reaction heat of  $NH_4SH$ . Both of the contributions of  $NH_3$  phase change and  $NH_4SH$  production are much smaller than that of  $H_2O$  phase change. In the layer the thermal cooling is specified (140 – 200 km), the cooling is balanced by the sum of the advection term and the latent heating terms. The existence of a distinct layer of latent cooling just below the  $H_2O$  condensation level implies that the convection below is driven by cooling caused by  $H_2O$  evaporation and the heating from the lower boundary.

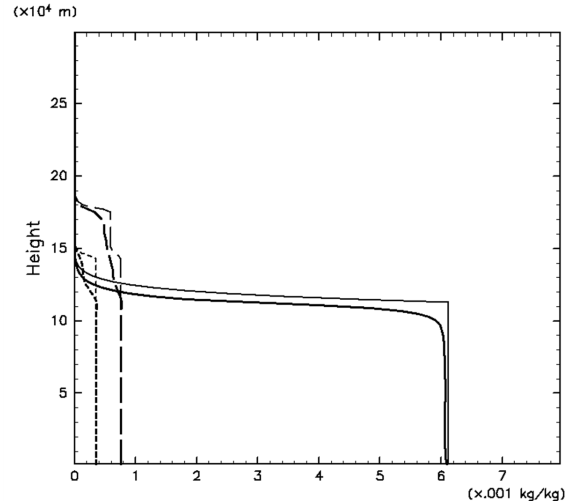


Figure 4. Vertical profiles of time and horizontal mean mixing ratio of condensible volatiles. Solid line means  $H_2O$  mixing ratio, broken line means  $NH_3$  mixing ratio, and dotted line means  $H_2S$  mixing ratio. Thick lines mean the profiles obtained by our simulation and thin lines mean the profiles calculated by an ECCM.

Fig.6 shows the vertical profile of the time and horizontal mean squared buoyancy frequency ( $N^2$ ). There is a distinct maximum of stability at the  $H_2O$  condensation level. This explains why the  $H_2O$  condensation level act not only as a compositional boundary but also as a dynamical boundary (see Fig.3, b, d). The stable layer results mainly from the decrease of the  $H_2O$  mixing ratio; the contribution of the temperature variation is relatively small. The stable layer that corresponds to the  $NH_4SH$  production is rather difficult to distinguish from that corresponds to  $H_2O$  condensation. There is a peak of stability which correspond to  $NH_3$  condensation, but its effect on the structure of convection is not significant (Fig.3, d). The stable layers associated with  $NH_3$  condensation and  $NH_4SH$  production are much weaker than those predicted by ECCMs. This is because steep decrease of mixing ratio does not develop around the levels of clouds formation (see Fig.4).

#### 4.2. Comparison among 0.1, 1, and $10 \times$ solar cases

In the  $0.1 \times$  solar case, Fig.7 shows that clouds spread more horizontally than that obtained by the  $1 \times$  solar case (Fig.3). The clouds are similar to stratus type clouds, not cumulus type clouds. However,  $H_2O$  and  $NH_4SH$  cloud particles are advected up to altitude above the  $NH_3$  condensation level. The convective motion is not separated at the  $H_2O$  condensation level (about  $z = 130$  km), and the downdrafts can bring dry air from the tropopause to the levels as deep as 30 bars level.

In the  $10 \times$  solar case, moist convection develops with distinct temporal intermittency shown by Fig.8 (c). In the periods of active cloud development (for example,  $t \sim$

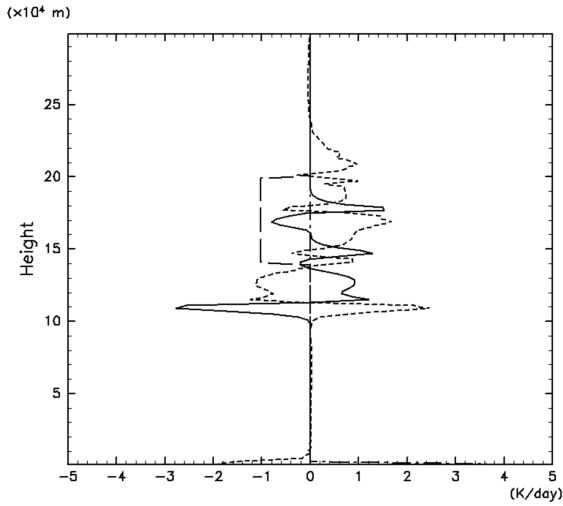


Figure 5. Time and horizontal mean thermal budget. Solid line represents the contribution of the latent heat of condensation (and evaporation) of  $H_2O$  and  $NH_3$  and the reaction heat of  $NH_4SH$ , dot-dashed line represents the contribution of heating at the bottom boundary, and dotted line represents the contribution of advection.

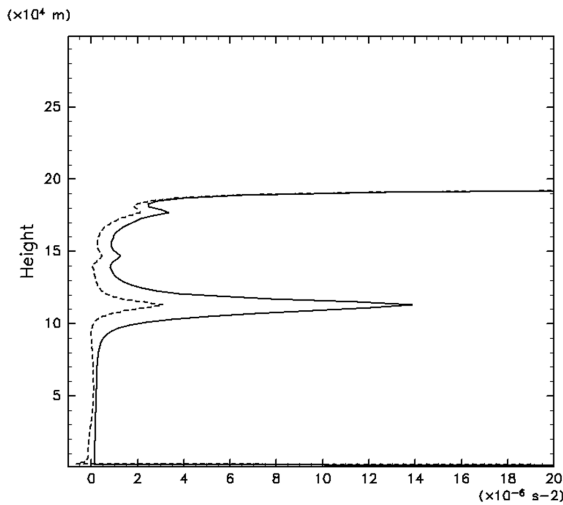


Figure 6. Vertical profile of the time and horizontal mean squared buoyancy frequency (solid line), and the contribution of the temperature variation (dotted line) in it. The difference between solid line and dotted line represents the contribution of the mixing ratios variation.

1060, 1210 hour of Fig.8, c), the distribution of clouds, condensable volatiles, potential temperature anomaly, and vertical velocity (not shown here) are similar to those obtained by the  $1 \times$  solar case (Fig.3). In the quiet periods, on the other hand, Fig.9 shows that clouds distribution are characterized with the two separate cloud layers. The lower one consists of  $H_2O$  and  $NH_4SH$  cloud particles,

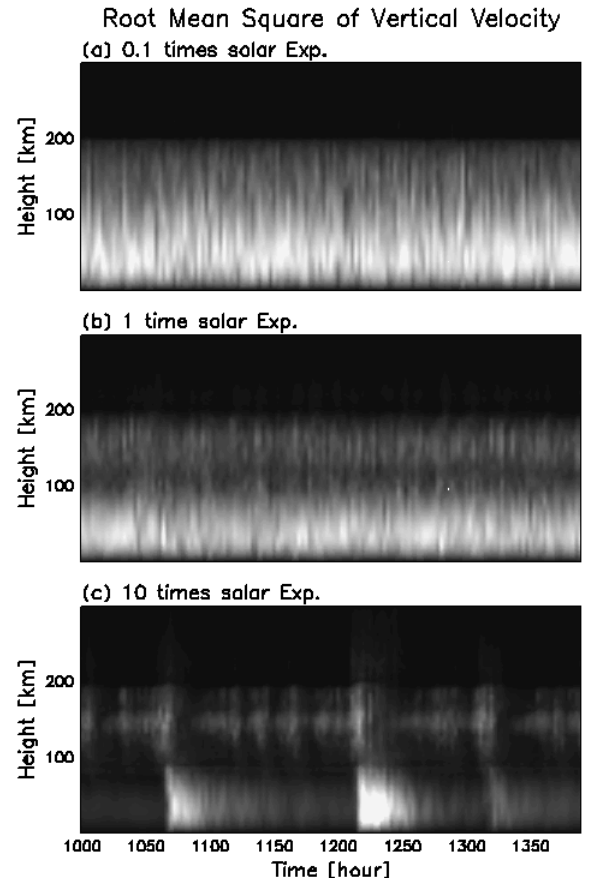


Figure 8. Time evolution of root mean square of vertical velocity for  $0.1 \times$  solar case (a),  $1 \times$  solar case (b), and  $10 \times$  solar case (c).

and the higher one is composed only of  $NH_3$  cloud layer. The vertical motions mainly occur between the bottom of cooling layer ( $z = 140$  km) and  $NH_3$  condensation level (about  $z = 170$  km), and the vertical motions below the  $H_2O$  condensation level is very weak.

Gross vertical structure of convective motion is compared in Fig.8, where the time evolution of root mean square of vertical velocity  $\sqrt{w^2}$  for 0.1, 1, and  $10 \times$  solar cases. The existence of the layers of small  $\sqrt{w^2}$  found at  $z = 120$  km in Fig.8 (b) and  $z = 90$  km in Fig.8 (c) means that  $H_2O$  condensation level acts as a dynamical boundary in the 1 and  $10 \times$  solar cases. On the other hand, in the  $0.1 \times$  solar case, no significant minimum of  $\sqrt{w^2}$  is found between the bottom boundary and the tropopause (Fig.8, a). This means that the stability at the  $H_2O$  condensation level in this case is not strong enough to prevent vertical motions.

Time and horizontal mean cloud mixing ratios are shown by Fig.10. Not only in snapshots (Fig.3, a) but also in the space time average, considerable amounts of  $H_2O$  and  $NH_4SH$  cloud particles exist above the  $NH_3$  condensation level in all cases.

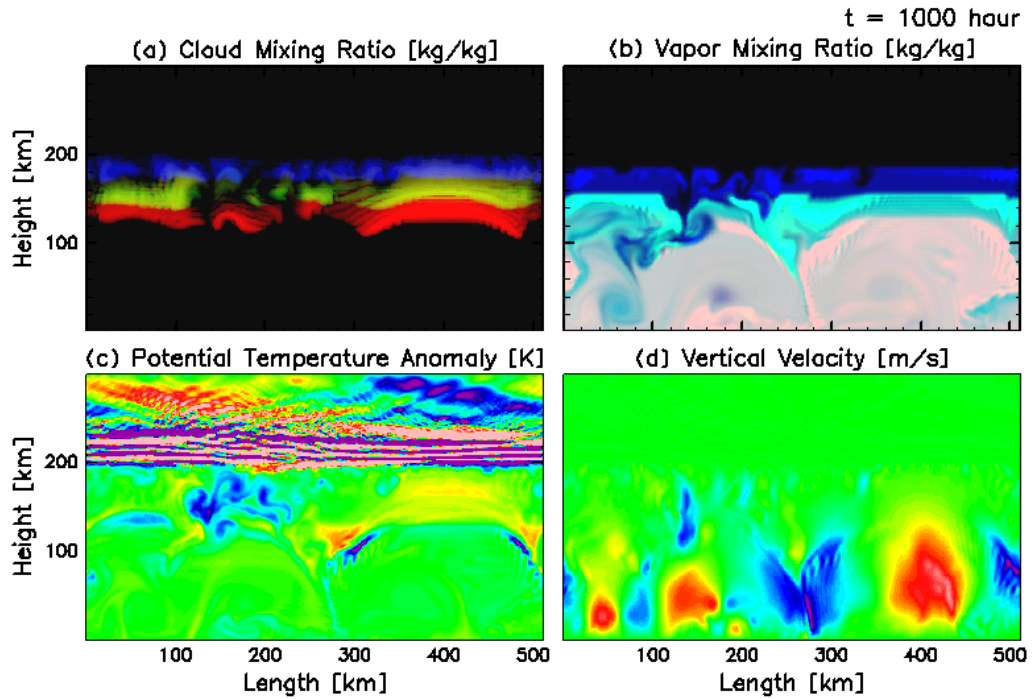


Figure 7. Same as Fig.3, but for the  $0.1 \times$  solar case. Note that potential temperature anomaly is represented by linear scale ranging from  $-0.5$  to  $0.5$  K.

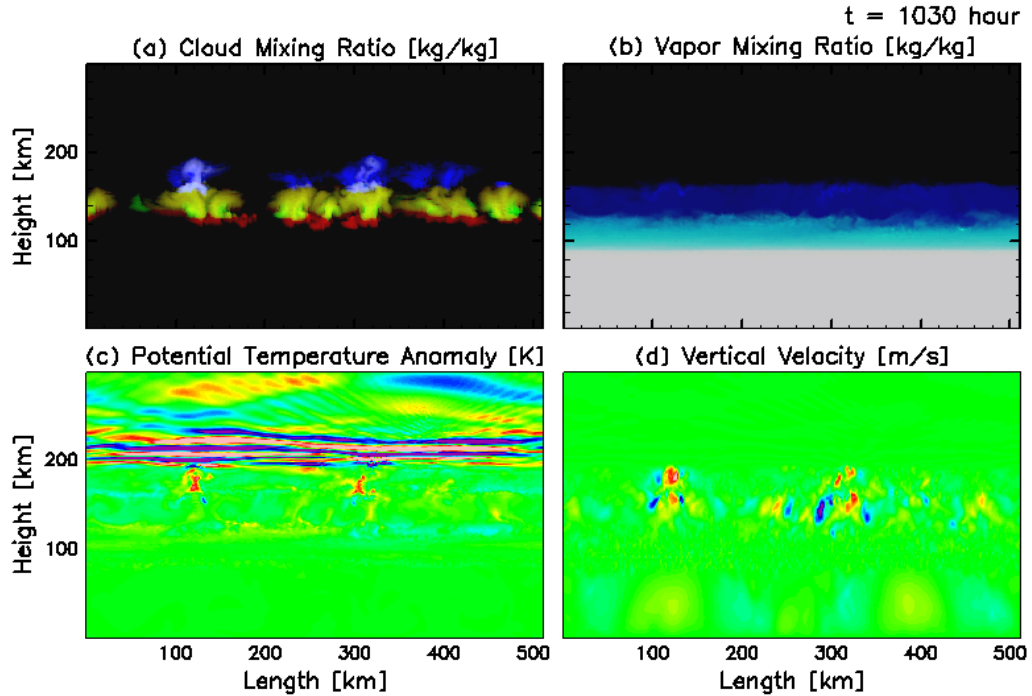


Figure 9. Same as Fig.3, but for the  $10 \times$  solar case. Snapshot of simulated cloud mixing ratios (a) and vertical velocity (b) are in quiet period. Note that vertical velocity is represented by linear scale ranging from  $-30$  to  $30$  m/s.

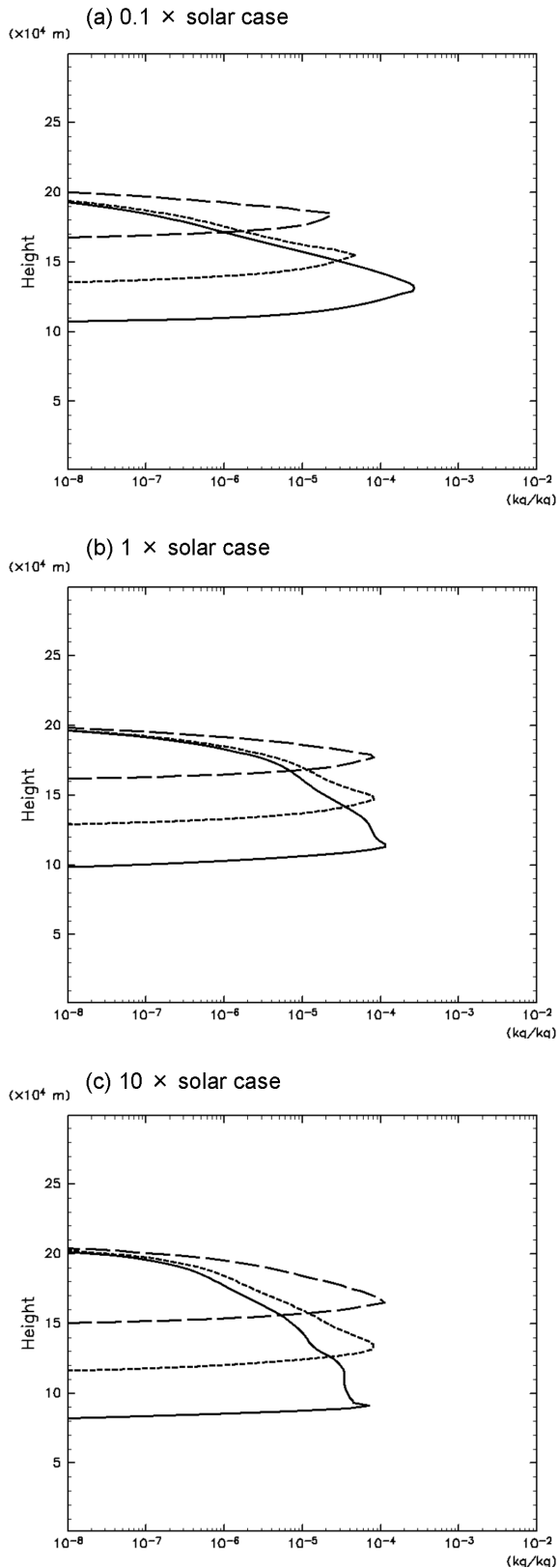


Figure 10. Time and horizontal mean mixing ratios of clouds for  $0.1 \times$  solar case (a),  $1 \times$  solar case (b), and  $10 \times$  solar case (c). Solid line means  $\text{H}_2\text{O}$  cloud mixing ratio, dotted line means  $\text{NH}_4\text{SH}$  cloud mixing ratio, and broken line means  $\text{NH}_3$  cloud mixing ratio.

## 5. Summary and suggestions for future Jupiter probe mission

In the present numerical experiments, considerable amounts of  $\text{H}_2\text{O}$  and  $\text{NH}_4\text{SH}$  clouds are advected to the altitudes above the  $\text{NH}_3$  condensation level. The characteristics of the profiles of clouds distinctly different from the classical three layers structure that has been expected by using equilibrium cloud condensation models.

The structure and the dynamics of the atmosphere strongly depend on the mixing ratios of condensible species in the deep troposphere. In the cases with standard or enhanced amount of condensible species,  $\text{H}_2\text{O}$  condensation level acts as a dynamical and compositional boundary; the region below  $\text{H}_2\text{O}$  condensation level is homogeneously wet. On the other hand, in the case with small amounts of condensible species, localized downdrafts frequently bring dry air from the tropopause to the levels as deep as 30 bars level. This dependency on the abundance of condensible species suggests two contrasting scenarios that can explain the dry condition observed by Galileo Probe. If Jupiter's deep atmosphere is rather depleted (e.g.,  $0.1 \times$  solar) in condensible components, ordinary thermal (or cloud) convection can entrain very dry air down to deep levels (e.g. 30 bar) and can easily explain the Galileo results. On the other hand, if Jupiter's deep atmosphere is wetter, the effect of motions other than cloud convection (e.g. large scale wave disturbances) is required.

Our numerical results predict that 1) cloud particles in the region of active moist convection consist of various mixtures of  $\text{NH}_3$ ,  $\text{NH}_4\text{SH}$ , and  $\text{H}_2\text{O}$ , 2) the horizontal distribution of condensible gasses is fairly inhomogeneous even in the layer below the condensation level of  $\text{H}_2\text{O}$  when the deep atmospheric each abundance of condensible volatiles is  $0.1 \times$  solar. In order to verify item 1), instruments that can determine not only the amounts but also the composition of cloud particles are desired to be developed. In order to consider item 2), a mission with multiple probes that descend various but rather adjacent locations is desired. Measurements of both average and spatial variability of the atmospheric composition especially under the cloud layer must be informative. Measurements of the composition, concentration, and size distribution of aerosol particles are also highly desired. These information are indispensable for modeling the unknown cloud microphysical processes.

Calculations with thermal forcing whose strength is close to that of the real radiative cooling in Jupiter's troposphere are in progress. A preliminary result shows that the results presented don't change qualitatively.

## Acknowledgement

Computations are done in NEC SX-6 at the PLanning and Information center of ISAS/JAXA, Japan, and on SR-11000 at the Computing and Communication Center, Hokkaido University, Japan. The authors would like to thank M. Yamada for his idea of visualization, M. Ishiwatari, K. Kuramoto, and S. Watanabe for their useful comments. This research is supported by the grant-in-aid for basic research from the ministry of education, culture,

cience and technology, Japan.

## References

- [1] Gierasch, P.J., Ingersoll, A.P., Banfield, D., Ewald, S.P., Helfenstein, P., Simon-Miller, A.A., Vasavada, A.R., Breneman, H.H., Senske, D.A., and the Galileo Imaging Team (2000) *Nature*, **403**, 628–630 (2000)
- [2] Ingersoll, A.P., Gierasch, P.J., Banfield, D., Vasavada, A.R., and Galileo Imaging Team (2000) *Nature*, **403**, 630–632
- [3] Weidenschilling, S.J. and Lewis, J.S. (1973) *Icarus*, **20**, 465–476
- [4] Atreya, S.K. and Romani, P.N. (1985) *Recent Advances in Planetary Meteorology*, 17–68, Cambridge Univ. Press, London
- [5] Yair, Y., Levin, Z., and Tzivion, S. (1995) *Icarus*, **114**, 278–299
- [6] Hueso, R. and Sanchez-Lavega, A. (2001) *Icarus*, **151**, 257–274
- [7] Asplund, M., Grevesse, N., and A. J. Sauval., *ASP Conference Series*, **336**, 25–38
- [8] Sugiyama, K., Odaka, M., Kuramoto, K., and Hayashi, Y.-Y. (2006) *Geophys. Res. Lett.*, **33**, L03201, doi:10.1029/2005GL024554
- [9] Nakajima, K., Takehiro, S., Ishiwatari, M., and Hayashi, Y.-Y. (2000) *Geophys. Res. Lett.*, **27**, 3129–3133
- [10] Klemp J. B. and Wilhelmson, R. B. (1978) *J. Atmos. Sci.*, **35**, 1070–1096
- [11] Kessler, E. (1969) *Meteor. Monogr.*, **32**, pp.84
- [12] Stromovsky, L. A., Collard, A. D., Fry, P. M., Orton, G. S., Lemmon, M. T., Tomasko, M. G., and Freedman, R. S. (1998) *J. Geophys. Res.*, **103**, 22,929–22,978